Simultaneous Thermal and Electrical Analysis of Nonlinear Microwave Circuits

Vittorio Rizzoli, *Senior Member, IEEE,* Alessandro Lipparini, Vittorio Degli Esposti, Franco Mastri, and Claudio Cecchetti

Abstract—**The paper introduces a new software tool for the simultaneous determination of the thermal and electrical steady-state regimes of nonlinear microwave circuits containing temperature-dependent active devices. The analysis technique is an extension of the classic piecewise harmonic-balance method, and is quite general-purpose. It can be applied to networks operating under multiple-tone excitation, including pulsed-RF regimes. The simulation problem is reduced to a nonlinear algebraic solving system whose unknowns are electrical and thermal state-variable harmonics. Advanced numerical techniques are used to effectively overcome the difficulties arising from the high degree of nonlinearity and from the very large number of unknowns of the numerical problem. The program incorporates a facility for the evaluation of the thermal constants of multiple-finger planar devices starting from geometrical data.**

I. Introduction

In THE computer-aided design of microwave circuits, especially power circuits, the prediction of the active device operating temperatures represents a major concern. The theoretical research on this subject is usually aimed at the determination of the temperature distribution inside an active device under dc (or CW) operating conditions (e.g., [1]–[3]). From this kind of analysis, or alternatively from suitable measurement procedures (e.g., [4]), one obtains the peak temperature in the device (e.g., the channel temperature in a microwave FET), which is used to compute the device thermal resistance [3].

For periodically driven circuits (CW or single-tone operation), it is usually safe to assume that the steady-state device temperatures are time independent, because the thermal time constants are large with respect to the RF period. In some cases, especially in class-A operation, the knowledge of a device thermal resistance may then provide a rough *a priori* estimate of its peak operating temperature, making use of the expected bias point and power-added efficiency. In turn, this estimate may be used to adjust the temperature-dependent parameters of the device equivalent circuit. The situation is much more complicated in class-AB or class-C operation, since then the actual bias point is determined by nonlinear effects, such as rectification, and is not *a priori* known. Further difficulties arise under multitone excitation, since some of the intermodulation (IM) products may have very long periods. As a typical example, in pulsed-RF conditions each active device undergoes a thermal cycle which may have a major influence on the circuit performance, but obviously cannot be simply estimated. In all such cases the analysis must include the search for the (possibly time-dependent) unknown temperatures.

In this paper we introduce a novel CAD tool for the simultaneous determination of the electrical regime and the peak device temperatures in a nonlinear microwave circuit containing temperature-dependent devices and driven by multitone signals, including the pulsed-RF case. The electrical behavior of each nonlinear device is described by generalized parametric equations including temperature among the state variables, and the thermal behavior is characterized by a thermal resistance and a thermal time constant. The thermal parameters of multiple-finger planar devices are evaluated starting from layout information, so that the transient thermal properties of such devices can be directly related to their geometries. As an example, a rigorous computation of the so-called "thermal impedance" [5] of a power device (depending on pulse width) becomes straightforward in this way. This new simulation capability thus represents a significant step in the development of a general-purpose process-oriented microwave CAD system.

The method of analysis presented in the paper is an extension of the well-known piecewise harmonic-balance (HB) technique based on circuit decomposition. In steady-state multitone operation, both the temperatures and the electrical signals may be represented by multidimensional truncated Fourier expansions. With the harmonic-balance approach, the coefficients of such expansions represent the problem unknowns. Since the device equations are temperature-dependent, and in turn the device temperatures depend on the voltages and currents at the device ports through the internally dissipated powers, all these unknowns are coupled and must be determined by the nu-

Manuscript received October 26, 1991; revised January 14, 1992. This work was partly sponsored by the Italian Ministry of University and Scientific Research (MURST) and by the Istituto Superiore delle Poste e delle Telecommunicazioni (ISPT).

V. Rizzoli, A. Lipparini, and V. Degli Esposti. are with the Dipartimento di Elettronica, Informatica e Sistemistica, Universita Degli Studi di Bologna, Villa Griffone, 40044, 40136 Pontecchio Marconi, Bologna Italy.

F. Mastri is with the Istituto di Elettrotecnica, University of Bologna, Via Risorgimento 2, 40136 Bologna, Italy.

C. Cecchetti is with Fondazione Ugo Bordoni, Villa Griffone, 40044 Pontecchio Marconi, Bologna, Italy.

IEEE Log Number 9108327.

merical solution of a unique nonlinear algebraic system. The evaluation of the device thermal parameters is based on the well-known equivalence between the temperature field and the potential distribution in a microstrip structure [6]. The general extension of the harmonic-balance technique to thermal aspects is covered in Section II of the paper. This section also addresses the efficient solution of the nonlinear system by a Newton–Raphson method based on the exact computation of the Jacobian matrix. Section III is more specifically devoted to a discussion of the pulsed-RF analysis of power circuits. The same section also shows that the physical nature of the pulsed-RF problem allows the harmonic-balance equations to be effectively decoupled, so that this class of simulations can be effectively handled on ordinary workstations in spite of their large numerical sizes. Finally, Section IV describes the computation of the thermal parameters of a power device, and presents the analysis of a FET amplifier circuit for illustrative purposes.

II. The Harmonic Balance Technique

A. Formulation of the Problem

Let us consider a nonlinear microwave circuit operating in a quasi-periodic electrical regime generated by the intermodulation of F sinusoidal tones of incommensurable fundamental angular frequencies ω_i. Any signal $a(t)$ supported by the circuit may be represented by the multiple Fourier expansion

$$a(t) = \sum_{k \in S} A_k \exp(j\Omega_k t) \tag{1}$$

where Ω_k is a generic IM product of the fundamentals, i.e.,

$$\Omega_k = \sum_{i=1}^{F} k_i \omega_i = \boldsymbol{k}^T w_v \tag{2}$$

In (1), (2) k_i is an integer harmonic number, $\boldsymbol{k}$ is an F-vector of harmonic numbers, and w_v is the F-vector of the fundamentals. The vector $\boldsymbol{k}$ in (2) spans a finite subset $\boldsymbol{S}$ of the $\boldsymbol{k}$-space (containing the origin) which will be conventionally named the *signal spectrum*. The Fourier coefficient A_k will be named the *harmonic* of $a(t)$ at Ω_k (or the k-th harmonic of $a(t)$). Since we want the signal (1) to be real, $\boldsymbol{S}$ must be symmetric with respect to the origin, and $A_{-k} = A_k^*$. We shall also denote by $\boldsymbol{S}^+$ the subset of $\boldsymbol{S}$ such that $\Omega_k \geq 0$ for $\boldsymbol{k} \in \boldsymbol{S}^+$.

Let the nonlinear subnetwork be described by the generalized parametric equations [7]

$$\boldsymbol{v}(t) = \boldsymbol{u}\left[\boldsymbol{x}(t), \frac{d\boldsymbol{x}}{dt}, \cdots, \frac{d^n\boldsymbol{x}}{dt^n}, \boldsymbol{x_D}(t), \boldsymbol{T}(t)\right]$$

$$\boldsymbol{i}(t) = \boldsymbol{w}\left[\boldsymbol{x}(t), \frac{d\boldsymbol{x}}{dt}, \cdots, \frac{d^n\boldsymbol{x}}{dt^n}, \boldsymbol{x_D}(t), \boldsymbol{T}(t)\right] \tag{3}$$

where $\boldsymbol{v}(t)$, $\boldsymbol{i}(t)$ are vectors of voltages and currents at the common ports, $\boldsymbol{x}(t)$ is a vector of *electrical state variables* (ESV) and $\boldsymbol{x_D}(t)$ is a vector of time-delayed electrical state variables, i.e., $x_{Di}(t) = x_i(t - \tau_i)$ with τ_i a time constant. All vectors of electrical quantities appearing in (3) have a same size n_d equal to the number of common (device) ports. $\boldsymbol{T}(t)$ is an M-vector of absolute temperatures measured at M suitable locations inside the nonlinear subnetwork. In the first application of this new methodology, we shall assume that the nonlinear subnetwork is a collection of M nonlinear devices ($M \leq n_d$) thermally isolated from one another, and that the entries of $\boldsymbol{T}$ may be identified with the peak temperatures in such devices. In turn, $\boldsymbol{T}(t)$ will be written in the form

$$\boldsymbol{T}(t) = T_0 + \underline{\Delta}\,\boldsymbol{T}(t) \tag{4}$$

where T_0 is a common room temperature which will be considered as *a priori* known, and $\underline{\Delta}\,\boldsymbol{T}(t)$ is the set of maximum excess temperatures reached inside the nonlinear devices. The entries of $\underline{\Delta}\,\boldsymbol{T}(t)$ represent the *thermal state variables* (TSV). In principle, when the circuit is driven by a multitone excitation such as a pulsed RF signal, each TSV (namely, $\Delta T_r(t)$, $1 \leq r \leq M$) is a quasi-periodic function of time of the form (1). In practice the thermal time constants of real devices are much longer than the RF period, so that only low-frequency components are usually sufficient for an adequate description of the temperature waveforms. Thus $\Delta T_r(t)$ will be represented by (1) with $\boldsymbol{S}$ replaced by a *thermal spectrum* $\boldsymbol{S_T} \subset \boldsymbol{S}$.

The quasi-periodic electrical regime of the nonlinear circuit resulting from a multitone excitation is completely defined by the set $\boldsymbol{x}(t)$ of electrical state variables and by the set $\underline{\Delta}\,\boldsymbol{T}(t)$ of thermal state variables. Because of (1), the state can be equivalently identified by the vectors $\boldsymbol{X}$, $\underline{\Delta}$ of the real and imaginary parts of the electrical and thermal state-variable harmonics, respectively. The entries of these vectors represent the problem unknowns. The total number of unknowns is $N_U = n_d n_S + M n_T$, where n_S is the number of lines of the signal spectrum, and n_T is the number of lines of the thermal spectrum. Performing a circuit simulation by the HB technique means finding these unknowns. To do so, we derive a nonlinear solving system by combining the usual requirement of vanishing *electrical harmonic-balance* (EHB) errors with the thermal equations of the nonlinear devices.

The linear subnetwork may be represented by the frequency-domain equation

$$\boldsymbol{Y}(\omega)\,\boldsymbol{V}(\omega) + \boldsymbol{N}(\omega) + \boldsymbol{I}(\omega) = \boldsymbol{0} \tag{5}$$

where $\boldsymbol{V}(\omega)$, $\boldsymbol{I}(\omega)$ are vectors of voltage and current phasors at the device ports, $\boldsymbol{Y}(\omega)$ is the linear subnetwork admittance matrix, and $\boldsymbol{N}(\omega)$ is a vector of Norton equivalent current sources. Thus the set of complex EHB errors at a generic IM product Ω_k has the expression

$$\boldsymbol{E}_{Ek}(\boldsymbol{X}, \underline{\Delta}) = \boldsymbol{Y}(\Omega_k)\,\boldsymbol{U}_k(\boldsymbol{X}, \underline{\Delta}) + \boldsymbol{N}(\Omega_k) + \boldsymbol{W}_k(\boldsymbol{X}, \underline{\Delta}) \tag{6}$$

where $\boldsymbol{U}_k$, $\boldsymbol{W}_k$ are the $\boldsymbol{k}$th harmonics of $\boldsymbol{u}(t)$, $\boldsymbol{w}(t)$. In order to avoid the use of negative frequencies, the nonlinear solving system is formulated in terms of a vector $\boldsymbol{H}_E$ of

real and imaginary parts of the EHB errors given by (6) for $\boldsymbol{k} \in \boldsymbol{S}^+$. Thus the electrical part of the solving system has the form

$$\boldsymbol{H}_E(\boldsymbol{X}, \underline{\boldsymbol{\Delta}}) = \boldsymbol{0}. \tag{7}$$

In the first application of this new analysis technique, we shall assume for simplicity that the thermal behavior of each device is fully characterized by a thermal resistance θ and by a thermal time constant τ_T. Thus the thermal equation of the generic (rth) device can be written

$$\tau_{Tr} \frac{d\,\Delta T_r}{dt} = -\Delta T_r(t) + \theta_r p_r(t) \tag{8}$$

where $p_r(t)$ is the instantaneous power dissipated in the device under consideration, namely

$$p_r(t) = \sum_j^{(r)} u_j(t) w_j(t). \tag{9}$$

The superscript (r) in (9) denotes that the summation is only extended to the ports belonging to the rth device.

We shall also assume that all devices are thermally linear (i.e., θ_r and τ_{Tr} are constants), though the simulation methodology introduced here could be easily extended to the case of temperature-dependent thermal parameters [8], [9]. Taking the (multiple) Fourier transform of (8) we can thus define the complex *thermal harmonic-balance* (THB) error for the rth device at Ω_k as

$$E_{Tr,k}(\boldsymbol{X}, \underline{\boldsymbol{\Delta}}) = \frac{\theta_r}{1 + j\Omega_k \tau_{Tr}} P_{r,k}(\boldsymbol{X}, \underline{\boldsymbol{\Delta}}) - \Delta_{r,k} \tag{10}$$

where $P_{r,k}$ and $\Delta_{r,k}$ are the $\boldsymbol{k}$th harmonics of $p_r(t)$ and $\Delta T_r(t)$, respectively. Note that the THB errors are easily computed through (3) and (9) as functions of the circuit state. At this stage we introduce a vector $\boldsymbol{H}_T$ of real and imaginary parts of all the errors (10) for $1 \le r \le M$ and $\boldsymbol{k} \in \boldsymbol{S}_T^+$. The complete nonlinear solving system thus takes the form

$$\begin{cases} \boldsymbol{H}_E(\boldsymbol{X}, \underline{\boldsymbol{\Delta}}) = \boldsymbol{0} \\ \boldsymbol{H}_T(\boldsymbol{X}, \underline{\boldsymbol{\Delta}}) = \boldsymbol{0}, \end{cases} \tag{11}$$

(11) is a system of N_U nonlinear real equations in N_U real unknowns, which can be solved by well-known numerical approaches, such as the Newton–Raphson method.

Note that the solution of (11) simultaneously provides the electrical regime of the nonlinear circuit (described by $\boldsymbol{X}$) and the time-dependent peak temperatures of the nonlinear devices (described by $\underline{\boldsymbol{\Delta}}$).

B. Exact Computation of the Jacobian Matrix

It is well established that the best performance of the Newton algorithm is obtained when the Jacobian of the nonlinear system can be evaluated by a theoretically exact algorithm rather than by numerical perturbations [10]. This has the twofold advantage of increasing both the speed and the robustness of the analysis algorithm (particularly for large-size jobs), because the Jacobian evaluation process becomes faster, and the derivatives more accurate. The computation of the exact Jacobian of (11) will be discussed in this section.

The Jacobian may be written

$$\boldsymbol{J} = \begin{bmatrix} \dfrac{\partial \boldsymbol{H}_E}{\partial \boldsymbol{X}} & \dfrac{\partial \boldsymbol{H}_E}{\partial \underline{\boldsymbol{\Delta}}} \\ \dfrac{\partial \boldsymbol{H}_T}{\partial \boldsymbol{X}} & \dfrac{\partial \boldsymbol{H}_T}{\partial \underline{\boldsymbol{\Delta}}} \end{bmatrix} \triangleq \begin{bmatrix} \boldsymbol{J}_{EE} & \boldsymbol{J}_{ET} \\ \boldsymbol{J}_{TE} & \boldsymbol{J}_{TT} \end{bmatrix}. \tag{12}$$

Both for ease of representation and for later convenience, the Jacobian is organized frequency-wise, i.e., is partitioned into submatrices, each containing the derivatives of the real and imaginary parts of the HB errors at a given mixing product, with respect to the real and imaginary parts of the SV harmonics at another mixing product. As an example, the generic submatrix of $\boldsymbol{J}_{EE}$ has the expression

$$\boldsymbol{J}_{EEk,s} = \begin{bmatrix} \dfrac{\partial \operatorname{Re}[\boldsymbol{E}_{Ek}]}{\partial \operatorname{Re}[\boldsymbol{X}_s]} & \dfrac{\partial \operatorname{Re}[\boldsymbol{E}_{Ek}]}{\partial \operatorname{Im}[\boldsymbol{X}_s]} \\ \dfrac{\partial \operatorname{Im}[\boldsymbol{E}_{Ek}]}{\partial \operatorname{Re}[\boldsymbol{X}_s]} & \dfrac{\partial \operatorname{Im}[\boldsymbol{E}_{Ek}]}{\partial \operatorname{Im}[\boldsymbol{X}_s]} \end{bmatrix} \tag{13}$$

where $\boldsymbol{X}_s$ is the set of complex ESV harmonics at Ω_s. From (6) we obtain, for $\boldsymbol{k}$, $\boldsymbol{s} \in \boldsymbol{S}^+$ and $\boldsymbol{t} \in \boldsymbol{S}_T^+$

$$\begin{aligned} \frac{\partial \boldsymbol{E}_{Ek}}{\partial f[\boldsymbol{X}_s]} &= \boldsymbol{Y}(\Omega_k) \frac{\partial \boldsymbol{U}_k}{\partial f[\boldsymbol{X}_s]} + \frac{\partial \boldsymbol{W}_k}{\partial f[\boldsymbol{X}_s]} \\ \frac{\partial \boldsymbol{E}_{Ek}}{\partial f[\underline{\boldsymbol{\Delta}}_t]} &= \boldsymbol{Y}(\Omega_k) \frac{\partial \boldsymbol{U}_k}{\partial f[\underline{\boldsymbol{\Delta}}_t]} + \frac{\partial \boldsymbol{W}_k}{\partial f[\underline{\boldsymbol{\Delta}}_t]} \end{aligned} \tag{14}$$

where the function $f[\cdot]$ may denote either the real or the imaginary part. The derivatives of the voltage and current harmonics $\boldsymbol{U}_k$, $\boldsymbol{W}_k$ are found in the following way. For the voltages (e.g.) we first introduce the multiple Fourier expansions

$$\begin{aligned} \frac{\partial \boldsymbol{u}}{\partial \boldsymbol{y}_m} &= \sum_{q \in S_{EE}} \boldsymbol{C}_{m,q} \exp(j\Omega_q t) \\ \frac{\partial \boldsymbol{u}}{\partial \boldsymbol{x}_D} &= \sum_{q \in S_{EE}} \boldsymbol{C}_q^D \exp(j\Omega_q t) \\ \frac{\partial \boldsymbol{u}}{\partial \boldsymbol{T}} &= \sum_{q \in S_{ET}} \boldsymbol{A}_q \exp(j\Omega_q t) \end{aligned} \tag{15}$$

where $\boldsymbol{y}_0 = \boldsymbol{x}$, $\boldsymbol{y}_m = d^m\boldsymbol{x}/dt^m$ $(1 \le m \le n)$, and $\boldsymbol{S}_{EE}$, $\boldsymbol{S}_{ET}$ will be named *derivatives spectra*. The derivation of the first of (3) now yields the derivatives of the voltage harmonics with respect to the state-variable harmonics ($\boldsymbol{k}$, $\boldsymbol{s} \in \boldsymbol{S}^+$, $\boldsymbol{t} \in \boldsymbol{S}_T^+$):

$$\begin{aligned} \frac{\partial \boldsymbol{U}_k}{\partial f[\boldsymbol{X}_s]} &= \sum_{m=0}^{n} f[1+j](j\Omega_s)^m [\underline{\boldsymbol{\Gamma}}_{m,k-s} + \{f[1+j]\}^2 \\ &\quad \cdot (-1)^m \underline{\boldsymbol{\Gamma}}_{m,k+s}] \\ \frac{\partial \boldsymbol{U}_k}{\partial f[\underline{\boldsymbol{\Delta}}_t]} &= f[1+j][\boldsymbol{A}_{k-t} + \{f[1+j]\}^2 \boldsymbol{A}_{k+t}] \end{aligned} \tag{16}$$

where

$$\underline{\Gamma}_{m,k-s} = \boldsymbol{C}_{m,k-s} + \delta_m^0 \boldsymbol{C}_{k-s}^D \exp(-j\Omega_s \tau) \quad (0 \le m \le n). \tag{17}$$

In (17) δ is Kronecker's symbol and τ is the diagonal matrix of the time delays. The vector summation index $\boldsymbol{q}$ in each of the derivatives (15) must span the entire set of values required in (16), where the combinations $\boldsymbol{k} \pm \boldsymbol{s}$ and $\boldsymbol{k} \pm \boldsymbol{t}$ appear. This explains the introduction of independent spectra for the derivatives. Similar expressions hold for the derivatives of the current harmonics. Equations (16) and (17) together with (14) allow a fast computation of $\boldsymbol{J}_{EE}$ and $\boldsymbol{J}_{ET}$. Note that $\boldsymbol{J}_{EE}$ coincides with the Jacobian matrix of a conventional HB analysis based on electrical state variables only [7].

In order to evaluate $\boldsymbol{J}_{TE}$ and $\boldsymbol{J}_{TT}$, we first gather all the complex errors (10) associated with a given IM product Ω_k into a vector of complex THB errors analogous to (6), namely

$$\boldsymbol{E}_{Tk}(\boldsymbol{X}, \underline{\boldsymbol{\Delta}}) = \boldsymbol{L}_k \boldsymbol{P}_k(\boldsymbol{X}, \underline{\boldsymbol{\Delta}}) - \underline{\boldsymbol{\Delta}}_k \tag{18}$$

where $\boldsymbol{P}_k$ and $\underline{\Delta}_k$ are the sets of kth harmonics of $p_r(t)$ and $\Delta T_r(t)$ for $1 \le r \le M$, respectively, and $\boldsymbol{L}_k$ is the diagonal matrix

$$\boldsymbol{L}_k = \operatorname{diag}\left[\frac{\theta_r}{1 + j\Omega_k \tau_{Tr}}\right] \quad (1 \le r \le M). \tag{19}$$

From (18) we obtain, for $\boldsymbol{k}$, $\boldsymbol{t} \in \boldsymbol{S}_T^+$ and $\boldsymbol{s} \in \boldsymbol{S}^+$,

$$\frac{\partial \boldsymbol{E}_{Tk}}{\partial f[\boldsymbol{X}_s]} = \boldsymbol{L}_k \frac{\partial \boldsymbol{P}_k}{\partial f[\boldsymbol{X}_s]}$$

$$\frac{\partial \boldsymbol{E}_{Tk}}{\partial f[\underline{\boldsymbol{\Delta}}_t]} = \boldsymbol{L}_k \frac{\partial \boldsymbol{P}_k}{\partial f[\underline{\boldsymbol{\Delta}}_t]} - f[1 + j]\, \delta_k^t \boldsymbol{I}_M \tag{20}$$

where $\boldsymbol{I}_M$ denotes an identity matrix of order M.

The key information required for the computation of (20) is thus represented by the derivatives of $\boldsymbol{P}_k$ with respect to both $\boldsymbol{X}_s$ and $\underline{\boldsymbol{\Delta}}_t$. These can be obtained in the following way. Let us temporarily denote by $\boldsymbol{y}$ any of the arguments of the device equations (3). From (9) we get

$$\frac{\partial p_r(t)}{\partial \boldsymbol{y}} \sum_j^{(r)} = \left(\frac{\partial u_j(t)}{\partial \boldsymbol{y}} w_j(t) + u_j(t) \frac{\partial w_j(t)}{\partial \boldsymbol{y}}\right) \tag{21}$$

The point here is that the samples of $\boldsymbol{u}$, $\boldsymbol{w}$, $\partial \boldsymbol{u}/\partial \boldsymbol{y}$, $\partial \boldsymbol{w}/\partial \boldsymbol{y}$, are already available as a result of the computation of $\boldsymbol{J}_{EE}$, $\boldsymbol{J}_{ET}$ (and in particular of the expansions (15)), so that the samples of (21) may be immediately found. Thus we can also compute the coefficients of the multiple Fourier expansions

$$\frac{\partial \boldsymbol{p}}{\partial \boldsymbol{y}_m} = \sum_{\boldsymbol{q} \in \boldsymbol{S}_{TE}} \boldsymbol{F}_{m,q} \exp(j\Omega_q t)$$

$$\frac{\partial \boldsymbol{p}}{\partial \boldsymbol{x}_D} = \sum_{\boldsymbol{q} \in \boldsymbol{S}_{TE}} \boldsymbol{F}_q^D \exp(j\Omega_q t)$$

$$\frac{\partial \boldsymbol{p}}{\partial \boldsymbol{T}} = \sum_{\boldsymbol{q} \in \boldsymbol{S}_{TT}} \boldsymbol{G}_q \exp(j\Omega_q t) \tag{22}$$

where $\boldsymbol{p}$ is the vector of the dissipated powers $p_r(t)$ ($1 \le r \le M$), and $\boldsymbol{S}_{TE}$, $\boldsymbol{S}_{TT}$ are suitable derivatives spectra. The required derivatives may now be expressed by equations similar to (16), (17):

$$\frac{\partial \boldsymbol{P}_k}{\partial f[\boldsymbol{X}_s]} = \sum_{m=0}^{n} f[1 + j](j\Omega_s)^m [\underline{\boldsymbol{\Phi}}_{m,k-s} + \{f[1 + j]\}^2 \cdot (-1)^m \underline{\boldsymbol{\Phi}}_{m,k+s}]$$

$$\frac{\partial \boldsymbol{P}_k}{\partial f[\underline{\boldsymbol{\Delta}}_t]} = f[1 + j][\boldsymbol{G}_{k-t} + \{f[1 + j]\}^2 \boldsymbol{G}_{k+t}] \tag{23}$$

where

$$\underline{\boldsymbol{\Phi}}_{m,k-s} = \boldsymbol{F}_{m,k-s} + \delta_m^0 \boldsymbol{F}_{k-s}^D \exp(-j\Omega_s \tau) \tag{24}$$

and $\boldsymbol{k}$, $\boldsymbol{t} \in \boldsymbol{S}_T^+$, $\boldsymbol{s} \in \boldsymbol{S}^+$.

III. Pulsed-RF Operation of Power Circuits

A. Analysis Approach

Let the nonlinear circuit be excited by an RF sinusoidal source of angular frequency ω_1 (*carrier*) modulated by a periodic signal $s(t)$ of period $2\pi/\omega_2$. For the applications of interest in this section, $s(t)$ is ideally a sequence of rectangular pulses, which for practical purposes is approximated by a truncated Fourier expansion with N harmonics. Thus we have

$$s(t) = \sum_{k_2=-N}^{N} S_{k_2} \exp(jk_2 \omega_2 t) \tag{25}$$

where $S_{-k_2} = S_{k_2}^*$. In agreement with (1), the unmodulated input signal is represented by

$$v(t) = 2 \operatorname{Re}[V_1 \exp(j\omega_1 t)] \tag{26}$$

so that the modulated excitation becomes

$$u(t) = v(t)s(t) = 2 \operatorname{Re}\left\{\sum_{k_2=-N}^{N} V_1 S_{k_2} \exp[j(\omega_1 + k_2 \omega_2)t]\right\}. \tag{27}$$

Exciting the circuit by the signal (27) is equivalent to applying at the RF input port $2N + 1$ sinusoidal sources of complex amplitudes $2V_1 S_{k_2}$ and frequencies $\omega_1 + k_2 \omega_2$ ($0 \le |k_2| \le N$) connected in series. It is thus clear that a pulsed-RF analysis can be treated by the harmonic-balance technique as a special case of multitone excitation. The exciting frequencies $\omega_1 + k_2 \omega_2$ can be viewed as intermodulation products of two incommensurable fundamentals ω_1, ω_2, so that the problem defined by the excitation (27) is in fact a *two-tone* problem, with an unusually large number of harmonically related sinusoidal sources. Of course, this is only true when the sequence of pulses is periodic. However, if the pulse repetition time is long enough with respect to the thermal constants of the active devices, the results are also valid for isolated pulses (and for non-periodic sequences). Note that the modulation defined by (25) can be applied to the bias sources as well. In this case a dc source $E_0 S_0$ and N sinusoidal sources of complex amplitudes $2E_0 S_{k_2}$ at frequencies $k_2 \omega_2$ ($1 \le k_2$

$\leq N$) are connected in series to the bias port of interest (E_0 is the unmodulated bias voltage). This procedure may be used in the simulation of power circuits for which the input RF signal and the bias voltage are pulsed synchronously. Suitable definitions of the spectra are [11]

$$\boldsymbol{S} \triangleq \begin{cases} 0 \leq |k_1| \leq P \\ 0 \leq |k_2| \leq N \end{cases} \tag{28}$$

$$\boldsymbol{S_T} \triangleq \begin{cases} k_1 = 0 \\ 0 \leq |k_2| \leq N \end{cases} \tag{29}$$

yielding $n_S = (2P + 1)(2N + 1)$ and $n_T = 2N + 1$. Whenever the power circuit is strongly driven, it is essential that P be chosen as the number of carrier harmonics that have to be considered in the CW analysis of the same circuit. In such cases, the results of a simulation performed with $P = 1$ are grossly in error. As an example, the analysis of a FET power amplifier operating in the saturation region typically requires values of P ranging from 4 to 6. Thus any signal flowing in the circuit can be viewed as the superposition of $P + 1$ other signals, each consisting of a modulated carrier harmonic (including dc).

The most obvious approach to the approximation of the modulating waveform would be to use the truncated Fourier series for a sequence of ideal rectangular pulses. However, this solution is not acceptable for practical purposes because it does not allow the pulse rise and fall times to be controlled, and because of the large ripples occurring in the approximated waveform. Since the circuit response may exhibit ripples produced by distortion, it is essential that any spurious fluctuations occurring in the input signal be much smaller in magnitude, otherwise the results could be misinterpreted.

A possible way of overcoming these difficulties is to make use of a non-ideal pulse waveform of the kind shown in Fig. 1. The abrupt rise and fall at the beginning and at the end of the pulse are replaced by smooth transitions (e.g., of sinusoidal shape). The pulse rise and fall times (t_r, t_f) can thus be accurately defined as the times taken by the signal envelope to rise or fall between the 10% and 90% (e.g.) amplitude points [12]. Fig. 1 also shows the other parameters relevant to the definition of the pulse shape, i.e., the pulse width τ and the pulse repetition time T. The duty cycle is defined as τ/T. The ratios t_r/T, t_f/T essentially determine the number N of harmonics required to approximate the pulse shape with a prescribed maximum ripple, and thus have a major effect on the numerical cost of the simulation. Although a regular Fourier expansion of the train of pulses usually gives satisfactory results, the coefficients of (25) can also be numerically optimized in order to minimize the ripple. As an example, the sum of (25) with $N = 100$ is plotted in Fig. 2 for a sequence of pulses having a duty cycle of 10% and rise and fall times equal to 1% of T. In this case, the maximum deviation from the exact waveform is about 0.006, which can be reduced to 0.0051 by optimization.

With the spectrum defined by (28), the Fourier expansion of the current through a load resistor R has the form

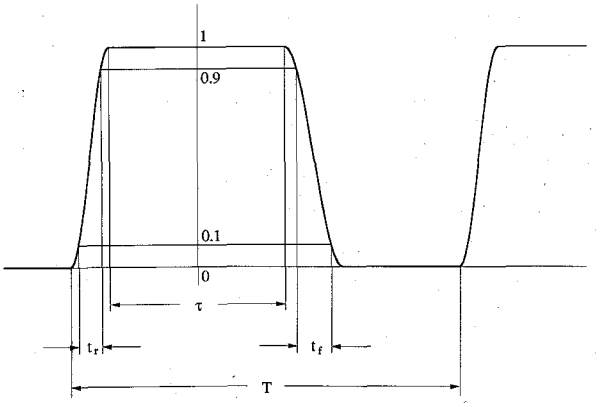

Fig. 1. Details of a realistic pulse waveform to be used in pulsed-RF analysis.

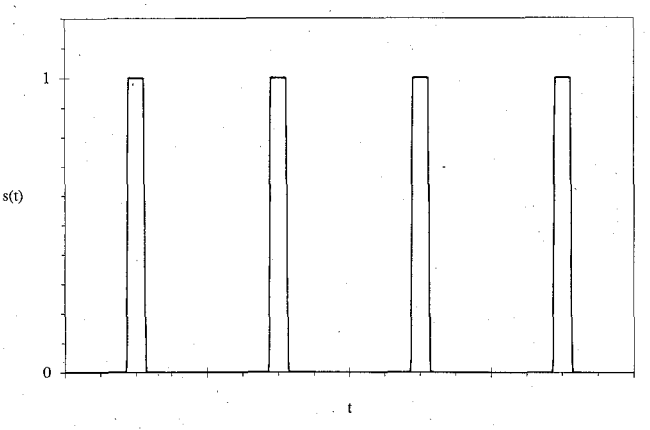

Fig. 2. Fourier approximation of a periodic sequence of rectangular pulses (duty cycle = 10%, rise and fall times = 1% of T).

$$i(t) = \sum_{k_1=-P}^{P} \sum_{k_2=-N}^{N} I_{k_1,k_2} \exp\left[j(k_1\omega_1 + k_2\omega_2)t\right] \tag{30}$$

where we write I_{k_1,k_2} for $I_{\boldsymbol{k}}$ ($\boldsymbol{k} = [k_1\, k_2]^T$). In the commonly encountered case of a modulating frequency much smaller than the carrier (e.g., $\omega_2 \leq 0.01\omega_1$), the quantity of primary interest is the power envelope $P(t)$ of the load current, defined as the time average of the instantaneous power $Ri^2(t)$ in a period of the carrier. From (30) by straightforward calculations we get

$$P(t) \cong R \sum_{k_1=-P}^{P} |a_{k_1}(t)|^2 \tag{31}$$

where

$$a_{k_1}(t) = \sum_{k_2=-N}^{N} I_{k_1,k_2} \exp\left(jk_2\omega_2 t\right). \tag{32}$$

The use of (31) through (32) allows the circuit response under pulsed-RF conditions to be displayed with a considerable saving of CPU time with respect to a straightforward use of (30).

B. Decoupling the Harmonic-Balance Equations

A straightforward application of the Newton-iteration based HB technique to pulsed-RF simulation may often be problematic at the workstation level, because the number of unknowns of the solving system may become quite large. It is obvious that the storage and factorization of the Jacobian by ordinary means are practically impossible when the number of unknowns exceeds some upper bounds depending on the computer system in use. As an example, let us consider a simple FET amplifier excited by a periodic train of pulses having the envelope shown in Fig. 1. As it was pointed out in the previous section, if it is desired to approximate the pulsed waveform with an accuracy better than 1%, we need to choose $N \cong 100$ in (28). Furthermore, for an accurate simulation of the saturated response of the amplifier, we need to consider at least $P = 4$ carrier harmonics. Thus the signal spectrum contains 1809 lines, the thermal spectrum contains 201 lines, and the total number of unknowns for this analysis is $N_U = 3819$. The storage of the full Jacobian then requires about 117 MB of memory in double-precision arithmetics, and its factorization is practically impossible on a typical workstation with 16 MB of central memory, because the time spent in transferring data to and from the virtual memory becomes virtually infinite.

An obvious way to overcome these difficulties would be to resort to large computer systems such as vector processors [10]. However, an in-depth investigation of the properties of the Jacobian matrix reveals the existence of an alternative procedure usable at the workstation level. In most practical cases of pulsed-RF operation, the modulating frequency ω_2 is several orders of magnitude smaller than the carrier ω_1. This often implies $N\omega_2 \ll \omega_1$; furthermore, the harmonics of the spectrum (28) usually tend to drop rapidly as $|k_2|$ is increased. Thus, due to (1) and (2), all the signals supported by the circuit have a fast time dependence through $\omega_1 t$, and a slow time dependence through $\omega_2 t$. Let us now consider the Fourier series (15), (22) for the derivatives. If the time slot used to compute the time-domain samples is of the order of $2\pi/\omega_1$ (and thus much shorter than $2\pi/\omega_2$), the effects of the modulation are virtually negligible, and all the expansions (15), (22) only contain mixing products for which $k_2 = 0$. Assuming that in the same expansions only harmonics of ω_1 up to the Dth order are significant ($D \leq 2P$), we end up with the following determination of the derivatives spectra:

$$\boldsymbol{S}_{EE} = \boldsymbol{S}_{ET} = \boldsymbol{S}_{TE} = \boldsymbol{S}_{TT} \triangleq \boldsymbol{S}_d = \begin{cases} 0 \leq |k_1| \leq D \\ k_2 = 0 \end{cases} . \tag{33}$$

The submatrix of the Jacobian (of the form (13)) associated with the $\boldsymbol{k}$th and $\boldsymbol{s}$th mixing products, is given by (14) or (20). Thus, because of (16) or (23), it is a combination of the harmonics of (15), (22) of orders $\boldsymbol{k} \pm \boldsymbol{s}$, where $\boldsymbol{k}$, $\boldsymbol{s}$ belong either to the signal or to the thermal spectrum. Due to the second of (33), this submatrix vanishes unless $|k_2| = |s_2|$, because otherwise $\boldsymbol{k} \pm \boldsymbol{s} \notin \boldsymbol{S}_d$. Now let the harmonics be gathered into groups according to the value of $|k_2|$. Since any submatrix of the Jacobian associated with two harmonics belonging to different groups is zero, the Jacobian is reduced to a block-diagonal form, and the solution of the linear system required to compute the Newton update is reduced to the solution of a number of uncoupled systems of smaller size. Specifically, with the spectra defined by (28) and (29), instead of computing and factorizing a square matrix of size N_U, one has to compute and factorize one matrix of size $n_d(2P + 1) + M$, and N matrices of size $2[n_d(2P + 1) + M]$ each. Note that this implies a *linear* dependence of the analysis cost on the number N of harmonics used to approximate the pulse waveform (25). Thus the simulation of narrow pulses with fast rise and fall times becomes affordable in this way.

Assuming that the LU decomposition is carried out by a standard algorithm such as Gauss or Crout [13], so that the factorization time is $O(2n^3/3)$ where n is the matrix size, this approach usually leads to a dramatic increase of numerical efficiency. Since the storage is limited to the nonzero entries of the Jacobian, an equally important memory saving is also obtained. As an example, let us consider once again the above-mentioned pulsed-RF problem. With the indicated dimensions, the LU factorization time for the block-diagonal Jacobian is reduced by a factor of 10^4 with respect to the dense case, while the storage drops from 117 to about 1.2 MB. The numerical job thus falls well within the reach of a typical workstation: one Jacobian decomposition takes about 50 CPU seconds on a SUN SPARCstation 2 with 16 MB of central memory in double-precision arithmetics. Note that this procedure is conceptually equivalent to subdividing the nonlinear solving system (11) into a number of uncoupled smaller subsystems. However, this decoupling is actually operated on the derivatives only, so that the solution obtained is always exact, provided that convergence be achieved. On the other hand, since (33) does not simply represent a mathematical approximation, but rather a straightforward consequence of the physical nature of the problem, the power-handling capability of the block-diagonal Newton iteration is high. Power amplifiers operated in saturation under pulsed-RF excitation can be usually analyzed by this technique without convergence problems.

Finally, from (16), (23) and the first of (33) it is evident that the parameter D represents the maximum difference between the orders of any two harmonics that are considered coupled under the approximations (33). Thus if the mixing products belonging to each group are ordered for increasing values of k_1, the corresponding block subsystem is banded with bandwidth equal to D (in terms of submatrices of the form (13)). Thus a band-matrix solver can be used for each block subsystem, with a further performance increase. This fact can be useful in the case of complex topologies containing several nonlinear devices.

If $D = 2P$, all the block subsystems are dense. Note that for a fixed D, the analysis cost becomes a linear function of the number P of carrier harmonics, as well.

IV. Computation of Thermal Parameters and Examples

Let us consider a power device having a multiple-finger topology, e.g., a microwave FET with G gate strips of dimensions $L \times W$ and spacing S between consecutive fingers. The electrodes are deposited on a semiconductor substrate of thickness H and thermal conductivity κ. The back of the substrate coincides with the heat sink surface, and is assumed to be held at a constant temperature T_0. In order to compute the thermal resistance, we represent the active channels as heat sources having the shape of thin sheets of the same dimensions and positions as the gate metallizations [14]. Within the simplified approach to thermal analysis described in Section II, these sources are assumed to have a common temperature T_S representing the peak temperature inside the device. The thermal resistance is then defined as

$$\theta = \frac{T_S - T_0}{P_S} \tag{34}$$

where P_S is the thermal power delivered by the heat sources in steady-state conditions.

In order to compute (34), we make use of the well-known analogy between the temperature field inside the device and the potential distribution in a microstrip structure having the same geometry [1], [14]. The analogy is a consequence of the fact that both the temperature T and the potential ϕ satisfy the Laplace equation with constant boundary conditions. Note that the thermal power across a given surface is the flux of $-\kappa \nabla T$, and thus corresponds to the electric charge in the analogy, since the equivalent of κ is the dielectric constant ϵ. Thus the equivalent of the thermal resistance is the inverse capacitance. Specifically, let us consider a dielectric slab of thickness H and permittivity ϵ, with a ground plane on one side, and G metal patches (rectangular microstrip sections) having the same geometries as the FET active channels on the other. The air-dielectric interface is treated as a magnetic wall because the thermal conductivity of air is negligible in the thermal problem. With the strips held at the same potential, the static capacitance C with respect to ground is computed by the Green's function method [15]. Then the thermal resistance is given by

$$\theta = \frac{\epsilon}{\kappa C}. \tag{35}$$

The effects of a temperature-dependent thermal conductivity inside the chip can be easily accounted for, if required, by the Kirchhoff transform [3].

In order to find the thermal time constant, we first compute the device thermal capacitance γ, which for our present purposes is defined as the amount of heat required to raise the peak device temperature T_S by 1°K, in agreement with (8). The solution of the microstrip problem by the Green's function method [15] automatically provides an approximate evaluation of the potential distribution $\phi(P)$ inside the dielectric, and thus of the temperature distribution $T(P)$ inside the semiconductor chip. In principle, to obtain the thermal capacitance we carry out the same calculation twice, with the same heat sink temperature T_0, and source temperatures T_S differing by 1°K. If the difference between the two temperature distributions is denoted by $\delta T(P)$, by definition we have

$$\gamma = \int_V \rho c \, \delta T(P) \, dV \tag{36}$$

where ρ is the material density, c its specific heat, and V the chip volume. Note that $\delta T(P)$ can be more directly obtained as the temperature distribution generated by the boundary conditions $T_0 = 0$, $T_S = 1$. Finally, the thermal time constant is simply given by

$$\tau_T = \theta \gamma. \tag{37}$$

As an example, let us consider a 2.4 mm GaAs FET with 0.5 μm gate length and a 12 gate geometry. Let the gate spacing be 40 μm and the chip thickness 75 μm. The capacitance of the associated microstrip structure is about 0.093 pF for $\epsilon_r = 10$. Making use of the typical value $\kappa \cong 0.038$ W/mm°K [16] for the thermal conductivity of gallium arsenide, (35) yields $\theta \cong 25$°K/W. Assuming $\rho \cong 5.32$ g/cm^3, $c \cong 0.325$ J/g°K [16], and a chip size of $0.7 \times 0.6 \times 0.075$ mm, from (36) we obtain $\gamma \cong 4.80 \cdot 10^{-6}$ J/°K. Finally (37) gives $\tau_T \cong 120$ μs. Note that all these values are roughly in agreement with typical empirical data for a FET of comparable geometry [14].

Now let the same device be embedded in a power amplifier having the simple topology illustrated in Fig. 3. The FET is described by a modified Materka and Kacprzak model [17] with $I_{DSS} = 488$ mA. For illustrative purposes, the temperature dependence of the FET performance is simply modeled by changing the expression of the nonlinear drain current source in the following way [18]:

$$i_{DS}(T) = i_{DS}(T_R) \left[\frac{T_R}{T} \right]^{\alpha} \tag{38}$$

where T_R is a fixed reference temperature ($T_R = 290$°K for the present case) and $\alpha \cong 1$ [14]. Although a more refined model would be necessary for an accurate simulation, (38) is sufficient to demonstrate the performance of the analysis algorithm. The device is biased at 9 V, 244 mA for class-A operation. Under CW excitation at 9.7 GHz with a room temperature of 290°K, the circuit has a saturated output power of +30.4 dBm at the 4 dB compression level, for which the power-added efficiency reaches a maximum of about 38.7%. The associated gain is 7.4 dB. The peak device temperature in these operation conditions is about 320°K and is constant with time.

Now let the amplifier be excited by a 9.7 GHz sinu-

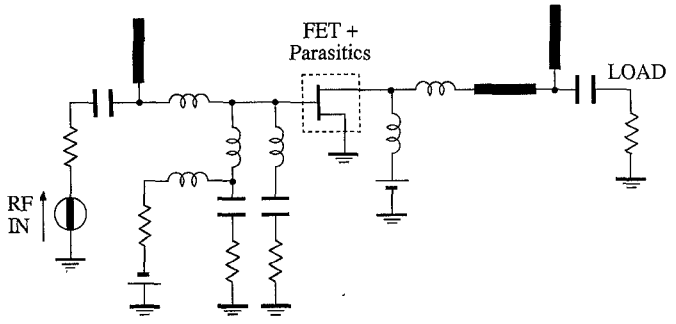

Fig. 3. Schematic topology of a microwave FET power amplifier.

soidal carrier modulated by a periodic sequence of rectangular pulses having a pulse repetition frequency of 1 kHz, and rise and fall times equal to 1% of the period. For HB analysis purposes, this waveform is approximated by a Fourier series with 100 harmonics, as it was discussed in Section III. The approximated modulating waveform is shown in Fig. 2 for a 10% duty cycle. The bias voltage is pulsed synchronously with the input signal, between 0 V and the nominal CW value of 9 V. Thus for a 10% duty cycle the bias signal waveform is still given by Fig. 2, with a different vertical scale. Referring to (28), $P = 4$ harmonics of the carrier are accounted for in the simulation, since this number is found to be sufficient for computing the transducer gain with a numerical accuracy of 0.1 dB in CW conditions. The size of the numerical problem then requires the use of the decoupling technique described in the preceding section. With this approach, the CPU time required for the pulsed-RF analysis on a SUN SPARCstation 2 with 16 MB of physical memory, is about 760 CPU seconds for a typical duty cycle of 30%, starting all harmonics from zero. This is quite acceptable given the problem complexity. Note that the analysis takes into account both the forward gate current and the drain-to-gate breakdown, as it is required for an accurate simulation of a power amplifier in the saturation region [19]. The adopted breakdown model is the empirical one proposed in [20].

Fig. 4 shows the power envelopes of the input and output pulses for the nominal peak input power level of +23 dBm (4 dB gain compression) and a 10% duty cycle. The pulse droop [12] produced by the temperature increase during the "on" state is evident in the output waveform. The signal and thermal spectra corresponding to the output waveform of Fig. 4 are given in Figs. 5 and 6. Fig. 7 shows the time dependence of the FET peak temperature for several values of the duty cycle, ranging from 50% down to 10%, and provides a comparison with the constant CW temperature. Note that the temperature swing within the pulse repetition period is found to drop quickly as the pulse duration is decreased below the thermal time constant (Fig. 7). Finally, in Fig. 8 the device *thermal impedance* [5] is plotted against the duty cycle. This quantity is defined here as the ratio between the maximum excess temperature reached inside the active device and the average power dissipated in it during the pulse "on" state.

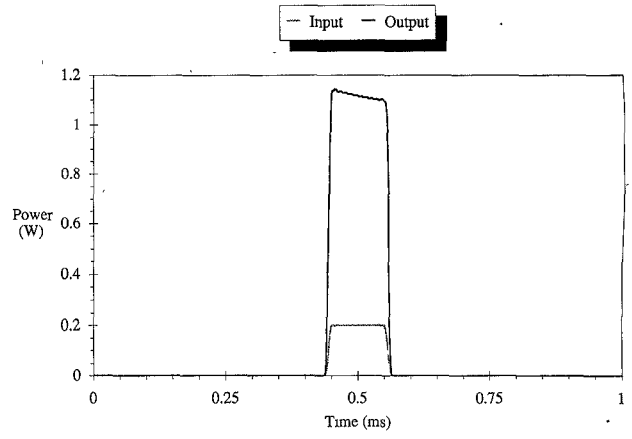

Fig. 4. Power envelopes of the input and output pulse waveforms for a pulse duty cycle of 10%.

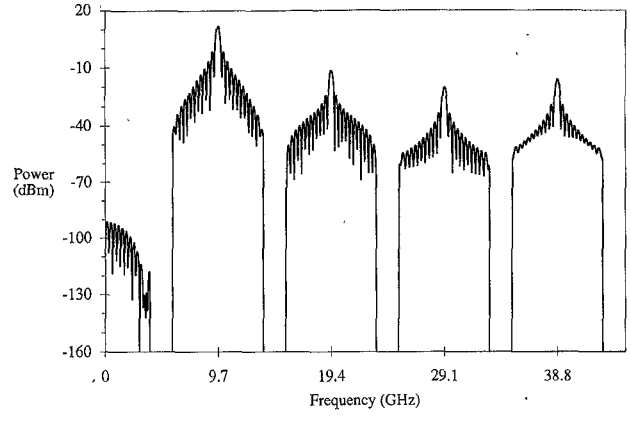

Fig. 5. Power spectrum of the output signal for a pulse duty cycle of 10%.

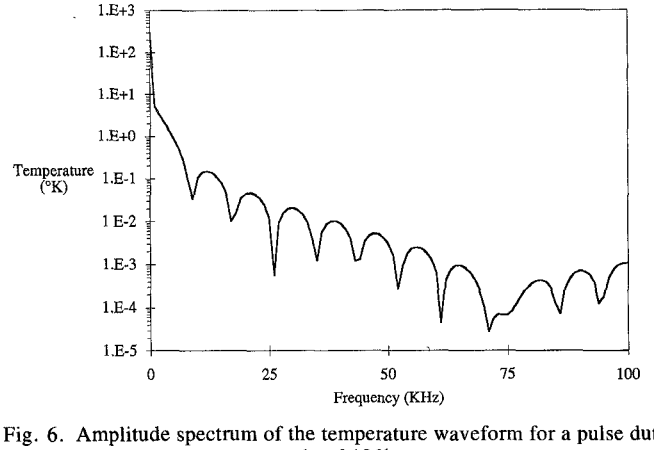

Fig. 6. Amplitude spectrum of the temperature waveform for a pulse duty cycle of 10%.

V. Future Developments and Conclusion

The paper has introduced a conceptually rigorous harmonic-balance approach to the computer-aided analysis of nonlinear microwave circuits containing temperature-dependent active devices, and an efficient numerical implementation of this approach. The algorithmic capabilities of the method have been demonstrated by presenting the coupled electrical and thermal analysis of a micro-

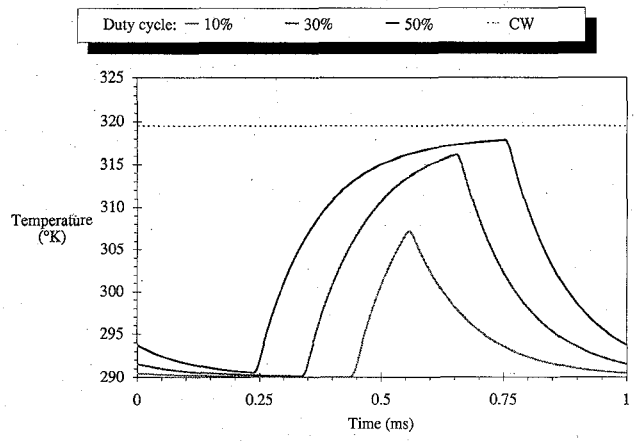

Fig. 7. Time-dependent peak temperature in the active device for several values of the pulse duty cycle. The median instants of the pulses are aligned at $t = 0.5$ ms.

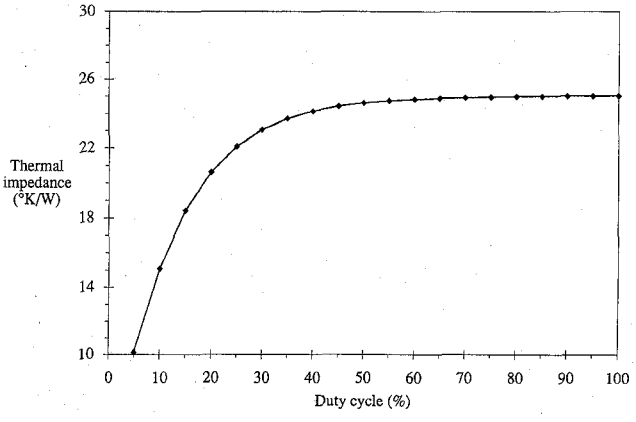

Fig. 8. Dependence of the device thermal impedance on the pulse duty cycle for a constant pulse repetition time ($T = 1$ ms).

wave power amplifier. To the authors' knowledge, a simulation tool of the same generality, including the ability to deal with pulsed-RF excitations, was not previously available. Thus the present work is likely to provide an important link between circuit- and process-oriented nonlinear CAD techniques. Since this work is essentially aimed at providing a proof of feasibility, several aspects of the problem have been considerably simplified. A number of refinements and developments are necessary for a full exploitation of the potential of this new analysis approach. These include, among others, accurate temperature-dependent equivalent circuits for the active devices, more refined models for the heat flow from the active devices to the ambient (e.g., includig a heat-sink model), and the consideration of the nonlinearity of the device thermal equations. Work on these subjects is currently in progress, and will be presented elsewhere.

References

[1] R. D. Lindsted and R. J. Surty, "Steady-state junction temperatures of semiconductor chips," *IEEE Trans. Electron Devices*, vol. ED-19, pp. 41–44, Jan. 1972.

[2] P. Leturcq *et al.*, "A new approach to thermal analysis of power devices," *IEEE Trans. Electron Devices*, vol. ED-34, pp. 1147–1156, May 1987.

[3] A. Haji-Sheikh, "Peak temperature in high-power chips," *IEEE Trans. Electron Devices*, vol. 37, pp. 902–907, Apr. 1990.

[4] H. Fukui, "Thermal resistance of GaAs field-effect transistors," in *1980 IEEE Int. Electron Devices Meeting Dig.*, Dec. 1980, pp. 118–121.

[5] A. Blicher, *Field-Effect and Bipolar Power Transistor Physics*. New York: Academic Press, 1981.

[6] R. C. Levine, "Determination of thermal conductance of dielectric-filled strip transmission line from characteristic impedance," *IEEE Trans. Microwave Theory Tech.*, vol. MTT-15, pp. 645–646, Nov. 1967.

[7] V. Rizzoli, C. Cecchetti, A. Lipparini, and F. Mastri, "General-purpose harmonic balance analysis of nonlinear microwave circuits under multitone excitation," *IEEE Trans. Microwave Theory Tech.*, vol. 36, pp. 1650–1660, Dec. 1988.

[8] M. N. Ozisik, *Heat Conduction*. New York: Wiley, 1980.

[9] R. S. Pengelly, *Microwave Field-Effect Transistors—Theory, Design and Applications*. Letchworth: Research Studies Press, 1986.

[10] V. Rizzoli *et al.*, "Modern perspectives in supercomputer-aided microwave circuit design," *Int. J. Microwave Millimeter-Wave Computer-Aided Engineering*, vol. 1, pp. 201–224, Apr. 1991.

[11] V. Rizzoli *et al.*, "Pulsed-RF and transient analysis of nonlinear microwave circuits by harmonic-balance techniques," in *1991 IEEE MTT-S Int. Microwave Symp. Dig.*, Boston, June 1991, pp. 607–610.

[12] E. D. Ostroff *et al.*, *Solid-State Radar Transmitters*. Dedham, MA: Artech House, 1985.

[13] G. H. Golub and C. F. Van Loan, *Matrix Computations*. Baltimore: Johns Hopkins University Press, 1989.

[14] J. V. DiLorenzo and D. K. Khandelval, *GaAs FET Principles and Technology*. Dedham, MA: Artech House, 1982.

[15] K. C. Gupta, R. Garg, and I. J. Bahl, *Microstrip Lines and Slotlines*. Dedham, MA: Artech House, 1979.

[16] *Properties of Gallium Arsenide*, INSPEC, Inst. Elec. Eng., EMIS Datareview series no. 2. Old Woking: The Gresham Press, 1986.

[17] A. Materka and T. Kacprzak, "Computer calculation of large-signal GaAs FET amplifier characteristics," *IEEE Trans. Microwave Theory Tech.*, vol. MTT-33, pp. 129–135, Feb. 1985.

[18] V. Rizzoli, A. Lipparini, and F. Mastri, "Harmonic-balance analysis of temperature-dependent nonlinear microwave circuits," in *Proc. 21st European Microwave Conf.* Stuttgart, Sept. 1991, pp. 1290–1295.

[19] R. J. Trew, "MESFET models for microwave CAD applications," *Int. J. Microwave Millimeter-Wave Computer-Aided Engineering*, vol. 1, pp. 143–158, Apr. 1991.

[20] C. Guo *et al.*, "Optimum design of nonlinear FET amplfiers," *IEEE Trans. Microwave Theory Tech.*, vol. MTT-35, pp. 1348–1354, Dec. 1987.

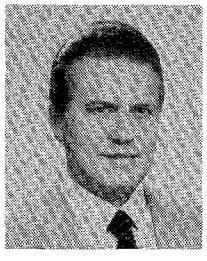

Vittorio Rizzoli (M'79–SM'90) received the degrees in electronic engineering from the University of Bologna, Italy. His thesis dealt with the computer-aided analysis of multistrip components for MIC's, with particular emphasis on the design criteria for interdigitated couplers.

From 1971 to 1973 he held a research grant issued by Fondazione Ugo Bordoni, and joined the Centro Onde Millimetriche in Pontecchio Marconi, Bologna, where he was involved in the development of IF circuitry for a millimeter-wave circular-waveguide communications system. In 1973 he was with the Stanford Park Division of the Hewlett Packard Company, Palo Alto, CA, where he was engaged in microwave transistor modeling and medium-power amplifier design. In 1974 he joined the University of Bologna, Italy, as an Associate Professor of Circuit Theory, and in 1980 he became a Full Professor of Electromegnetic Fields and Circuits. His teaching and research activities have been devoted to several topics, including the theory of electromagnetic propagation in optical fibers, and the simulation and design of passive and active microwave integrated circuits. More recently, he has been engaged in the development of algorithms and software tools for the computer-aided design of nonlinear circuits, and among others, he has developed the first general-purpose harmonic-balance simulator with optimization capabilities. He has authored or co-authored over 85 technical papers in the fields of electromagnetic propagation, microwave circuit CAD, and related subjects.

Mr. Rizzoli is a member of the Technical Committee MTT-1 on Computer-Aided Design, the editorial board of the IEEE TRANSACTIONS ON MICROWAVE THEORY AND TECHNIQUES, and of John Wiley's *International Journal of Microwave and Millimeterwave Computer Aided Engineering*. Since 1987, he has also been a member of the Technical Program Committee of the European Microwave Conference. In 1990–1991 he served as the Distinguished Microwave Lecturer of IEEE MTT-S for Region 8.

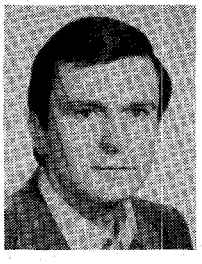

Alessandro Lipparini was born in Bologna, Italy, on August 31, 1947. He graduated with a degree in electronic engineering from the University of Bologna, Bologna, Italy, in 1974.

In 1974, he joined the Technical Staff of the Istituto di Elettronica, University of Bologna, as a Research Fellow. Since March 1975, he has been a Researcher for the Italian Ministry of Education at the University of Bologna, also serving as a Lecturer on Circuit Theory and Electromagnetic Field Theory. In 1987, he joined the University of Bologna as an Associate Professor of Electromagnetic Fields and Circuits. Since then, he has been teaching a course on microwave integrated circuits. His current research interests are in the field of MIC and MMIC with special emphasis on nonlinear circuits. He is also involved in a research project aimed at the development of vectorized software for microwave circuit design applications.

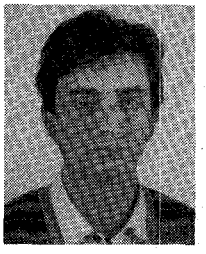

Vittorio Degli Esposti was born in Bologna, Italy, in 1964. He graduated in electrical engineering from the University of Bologna in March 1989.

From 1989 to 1990 he was with the Research Department of Siemens Telecomunicazioni, Milan, where he was involved in a research program on optical fiber high-speed communication systems. In 1990 he also joined the Technical Staff of the Dipartimento di Elettronica, Informatica e Sistemistica of the University of Bologna as a Research Fellow. Since November 1990 he attended the Electrical Engineering Ph.D. program at the University of Bologna. His main research interests are in the field of Applied Electromagnetics and in particular in the field of simulation and design of microwave circuits.

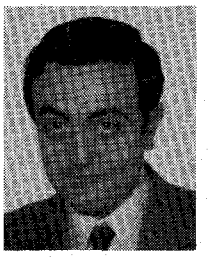

Franco Mastri was born in Forlì, Italy, in 1957. He received the degree in electronic engineering from the University of Bologna in 1985.

In 1987 and 1988 he obtained research grants issued by Fondazione Guglielmo Marconi, Pontecchio Marconi, Italy, and Selenia S.p.A., Rome, Italy to carry out a study on the application of nonlinear CAD techniques in MIC and MMIC design. In 1990 he joined the Istituto di Elettronica of the University of Bologna as a Researcher. His research interests are in the field of nonlinear circuits, with particular emphasis on numeric methods for circuit simulation.

Claudio Cecchetti was born in Forlì, Italy, in 1957. He received the degree in electronic engineering from the University of Bologna in October 1983.

In 1984–1985 he obtained a research grant issued by Fondazione G. Marconi, Pontecchio Marconi, Italy, to develop user-friendly interactive software for linear microwave circuits CAD. In 1985 he joined Fondazione U. Bordoni, Rome, Italy, where he is currently involved in research on nonlinear microwave circuits design. His main fields of interest are in the development of software tools for the simulation of several aspects of the nonlinear problem with special emphasis on frequency-domain techniques, including broadband circuit optimization, bipolar transistor modeling, transient analysis, thermal and noise effects.